Article

Oblique Projection-Based Covariance Matrix Reconstruction and Steering Vector Estimation for Robust Adaptive Beamforming

Yanliang Duan [ID], Yanping Gong, Xiaohui Yang and Weiping Cao *

Guangxi Key Laboratory of Wireless Wideband Communication & Signal Processing, Guilin University of Electronic Technology at Guilin, Guilin 541004, China
* Correspondence: weipingc@guet.edu.cn

Abstract: Adaptive beamforming can efficiently contract interference and noise. Due to high sensitivity of the beamformer to model mismatch, the capability of interference reduction will critically degrade when the signal model mismatch occurs, particularly when the sampling sequence contains the desired signal. For the purpose of enhancing the robustness of beamformers to signal model mismatch, we propose a new robust adaptive beamforming (RAB) method. Firstly, the precise steering vector (SV) associating with the desired signal is estimated by employing the minimum norm of subspace projection (MNSP) approach. Secondly, the nominal interference SVs are estimated via the maximum entropy power spectrum. Subsequently, the corrected interference SVs and powers are obtained by oblique projection. Finally, the interference-plus-noise covariance matrix (INCM) is reconstructed, and the proposed RAB is obtained. Multiple simulations are carried out and demonstrate the robustness of the proposed RAB method.

Keywords: robust adaptive beamforming; minimum norm of subspace projection; oblique projector; interference-plus-noise covariance matrix reconstruction

1. Introduction

Adaptive beamforming is a spatial filter which is designed to form directional beams to transmit or receive a desired signal from a designated direction, meanwhile attenuating interference signals from other directions. Adaptive beamforming has been widely used in wireless communication, microphone array speech processing, radar, sonar, medical imaging, radio astronomy and other areas [1]. The Standard Capon Beamformer (SCB) is an optimal spatial filter that maximizes the array output signal to the interference-plus-noise ratio (SINR), provided that the true covariance matrix and the signal steering vector are accurately known [2]. However, the existence of systematic model mismatch, such as array calibration error, finite snapshots, and others, is inevitable [1,3]. Adaptive beamformers are sensitive to model mismatch, especially when the desired signal is present in the sampling sequences [4]. Therefore, robust adaptive beamforming has been an intensive research topic, and various robust adaptive beamforming techniques have been proposed in the past decades [5].

Traditional RAB techniques include the diagonal loading (DL) technique and the eigenspace-based (ESB) technique [3,6]. The DL-based beamformers are derived by adding a scaled identity matrix on the sample covariance matrix (SCM) [3,7]. Although it has been proved to be effective in mitigating the effects of the finite sample size and SV mismatch [2,8], it is difficult to choose the optimal DL level in different scenarios [3]. Multiple methods were proposed in [2,9–11] to compute the DL levels automatically without specifying any additional user parameters [3]. However, these methods suffer from performance degradation at high signal-to-noise ratio (SNR) [12], which is a common problem with this category of method. The ESB beamformers are performed by projecting

the nominal SV onto an estimated subspace projector to mitigate the adverse impact caused by noisy disturbance [13–15]. The performance of the ESB beamformer is restricted at low SNR [8]. The author in [13] presents a modified ESB method which enhances the SCM for better performance, and a method in [15] adopts the knowledge of the signal angular region as a criterion to construct signal subspace. Although these methods lead to better performance at low SNRs, the problem of performance degradation aroused by large SV mismatches and high input SNRs appears. In [14], the proposed ESB method estimates the desired signal SV by adding an inequality constraint to an optimization problem, which exploits the orthogonality between the precise SV and noise subspace to ensure the validity of the estimation. This method is claimed to be effective in restraining arbitrary SV mismatch. However, there is still a common problem with ESB methods of low SNR performance degradation.

The uncertain-set-based technique utilizes a presumed spherical or ellipsoidal uncertainty set to constrain the signal SV mismatches and correct the nominal SV by solving an optimization problem [8]. The uncertain-set-based beamformers roughly include the following methods [6]: worst-case-based method [1,16], doubly constrained method [9,17], probabilistically constrained method [10,11] and linear programming method [18]. Compared with traditional DL methods, uncertainty-set-based methods are proposed based on clear theoretical analysis and thus have better robustness. Similar to the DL method, there is no reference criterion for the selection of the boundary of the uncertain-set. In fact, the uncertain-set technique transforms the DL level selection problem into an uncertain-set boundary selection problem. Therefore, the uncertainty-set-based method is essentially equivalent to a DL-based method or belongs to its extended class [19], and the uncertainty-set-based method is no longer valid when the SV mismatch is large or the precise SV mismatch does not locate in the presumed set [8,20].

The above methods mainly focus on correcting signal SV and enhancing the covariance matrix [21]. Since the desired signal component in the SCM is not eliminated [22], the above methods always suffer from performance degradation at high input SNRs [6]. To avoid this issue, the authors in [23] pioneer a novel RAB method called INCM reconstruction based method. This method has been proved to effectively eliminate the desired signal components. Gu modifies the above method in [5] and improves the performance, where the INCM is reconstructed by integrating over the complement of the desired signal angular region [6]. Unfortunately, this method performs poorly when the array calibration error exists in the systematic model, and the complexity of this method is very high. Authors in [4,24,25] represent multiple methods to reduce complexity. However, good performance can be obtained only in certain conditions. To resist multiple types of mismatches, authors construct a new constraint in [19] and add it to a QCQP optimization problem to estimate and correct the desired signal SV mismatch. For reducing INCM reconstruction errors, the residual noise is considered and eliminated from the Capon power spectrum estimator to reconstruct INCM and the desired signal SV more precisely in [7]. It is true that the incident signal may be covered by noise in the Capon power spectrum when the SV mismatch is large enough [6]. To overcome this drawback, the methods proposed in [26,27] substitute the Capon power spectrum with the maximum entropy power spectrum. Compared with [19], these methods can effectively reduce the complexity while maintaining good performance. Different from interference angular region integral-based or interference SV estimation-based INCM reconstruction RAB methods [6], the methods in [6,20,21] reconstruct INCM by using a subspace projection operation to filter out the desired signal component from the SCM. These methods achieve good performance with low complexity.

In this study, we propose a new INCM reconstruction-based RAB method [3]. Firstly, we estimate the desired signal SV via employing the MNSP approach. Secondly, we estimate nominal interference SVs via the maximum entropy power spectrum. Subsequently, we establish an oblique projection matrix based on the corrected desired signal SV and the signal subspace of the SCM to correct each interference nominal SV and power. Theoretical

analysis and multiple simulations are carried out to illustrate that the proposed RAB method performs well and can effectively combat various mismatches.

This paper is arranged into the following five sections. The necessary signal model and background associated with adaptive beamformer are described in detail in Section 2. In Section 3, the implementation step of this method is recounted in detail, including estimating the desired signal SV by MNSP and correcting the interference SV by oblique projection. In Section 4, multiple simulations and analysis are presented [28]. Finally, conclusions of the study are presented in Section 5. Acronyms used in this paper are las follow: robust adaptive beamforming (RAB), standard Capon beamformer (SCB), signal to interference-plus-noise ratio (SINR), direction of arrival (DOA), signal-to-noise ratio (SNR), interference-to-noise-ratio (INR), steering vector (SV), the minimum norm of subspace projection (MNSP), interference-plus-noise covariance matrix (INCM), sample covariance matrix (SCM), diagonal loading (DL), eigenspace-based (ESB), quadratically constrained quadratic programs (QCQP), uniform linear array (ULA), minimum variance distortionless response (MVDR), independently and identically distributed (i.i.d).

2. Signal Model and Background

Consider a half-wavelength-spaced ULA made up of M-omnidirectional-sensors [28]. L far-field uncorrelated narrowband signals, including one desired signal and $L-1$ interferences, illuminate the ULA [6,29]. The complex sampling sequences received by the ULA at k time-slot are expressed as [30]:

$$x(k) = x_s(k) + x_i(k) + x_n(k), \tag{1}$$

where $x_s(k) = s_0(k)a_0$ denotes an $M \times 1$ vector of the desired signal, $x_i(k) = \sum_{l=1}^{L-1} s_l(k)a_l$ denotes interference signal vector, and $s_l(k)$, $l = 0, \ldots, L-1$ denotes the lth signal vector, and its corresponding SV is a_l. $x_n(k)$ represents additive complex Gaussian noise with a zero mean and a variance of σ_n^2 [6]. The nominal SV associated with DOA θ can be written as:

$$
\begin{aligned}
a(\theta) &= \left[1, e^{-j\frac{2\pi d}{\lambda}sin\theta}, \ldots, e^{-j(M-1)\frac{2\pi d}{\lambda}sin\theta}\right]^T \\
&= \left[1, e^{-j\pi sin\theta}, \ldots, e^{-j(M-1)\pi sin\theta}\right]^T,
\end{aligned} \tag{2}
$$

where $(\cdot)^T$ represents the transpose operator, λ is the carrier wavelength, and d is the interelement spacing [31]. The output sequence of beamformer can be written as:

$$y(k) = w^H x(k), \tag{3}$$

where $w = (w_1, \ldots, w_M)^T$ is the complex weight vector of the beamformer [30], $(\cdot)^H$ represents the Hermitian transpose [32], and w can be calculated by maximizing the output SINR [6]. When precise σ_0^2 and a_0 is previously known, the definition of output SINR is formulated as follow:

$$SINR \triangleq \frac{\sigma_0^2 \left| w^H a_0 \right|^2}{w^H R_{i+n} w}, \tag{4}$$

where $E[\cdot]$ is the expectation operator of the stochastic variable [6]. The power of the desired signal is expressed as its mathematical expectation; that is; $\sigma_0^2 = E\left[|s_0(k)|^2\right]$, and the corresponding SV is a_0. $R_{i+n} \in \mathbb{C}^{M \times M}$ is precise INCM, and its definition is formulated as [31]:

$$
\begin{aligned}
R_{i+n} &= E\left\{ [x_i(k) + x_n(k)][x_i(k) + x_n(k)]^H \right\} \\
&= \sum_{l=1}^{L-1} \sigma_l^2 a_l a_l^H + E\left[x_n(k)x_n^H(k)\right] \\
&= R_i + \sigma_n^2 I,
\end{aligned} \tag{5}
$$

where $\sigma_l^2 = E\left[|s_l(k)|^2\right]$ is the lth interference power. $I \in \mathbb{R}^{M \times M}$, and σ_n^2 represents identity matrix and noise power. The maximization of (4) is equivalent to MVDR beamformer or called the Capon beamformer [33–35], and it is written as:

$$\min_{\boldsymbol{w}} \boldsymbol{w}^H \boldsymbol{R}_{i+n} \boldsymbol{w} \ \ s.t. \boldsymbol{w}^H \boldsymbol{a}_0 = 1. \tag{6}$$

The solution of the Capon beamformer is written as:

$$\boldsymbol{w}_{opt} = \frac{\boldsymbol{R}_{i+n}^{-1} \boldsymbol{a_0}}{\boldsymbol{a}_0^H \boldsymbol{R}_{i+n}^{-1} \boldsymbol{a_0}}. \tag{7}$$

Unfortunately, $\boldsymbol{R}_{i+n}$ and $\boldsymbol{a_0}$ cannot be obtained in practical scenarios. Therefore, they are usually replaced by the SCM $\hat{\boldsymbol{R}} = \frac{1}{K} \sum\limits_{k=1}^{K} \boldsymbol{x}(k) \boldsymbol{x}^H(k)$ with K sample snapshots and nominal SV $\bar{\boldsymbol{a}}_0$ [7].

It has been proved that replacing $\boldsymbol{R}_{i+n}$ by the SCM $\hat{\boldsymbol{R}}$ does not change the optimal output SINR [6]. At this point, the optimal weight vector becomes the sample covariance inversion (SMI) beamformer [7]:

$$\boldsymbol{w}_{SMI} = \frac{\hat{\boldsymbol{R}}^{-1} \bar{\boldsymbol{a}}_0}{\bar{\boldsymbol{a}}_0^H \hat{\boldsymbol{R}}^{-1} \bar{\boldsymbol{a}}_0}. \tag{8}$$

The SCM $\hat{\boldsymbol{R}}$ converge to the precise one only when $K \to \infty$. Due to the mismatches of $\bar{\boldsymbol{a}}_0$ and $\hat{\boldsymbol{R}}$, the performance of the SMI beamformer will severely deteriorate, especially in the case of high SNR [33,36].

3. Proposed RAB Method

In this section, the implementation steps of our proposed method are described in detail. For deriving optimal weight vector, reconstructed INCM and the estimated desired signal SV need to be obtained first [37]. The desired signal SV is estimated via employing the MNSP approach [37]. The INCM is reconstructed by two steps: interference DOAs estimation and interference SVs and powers correction.

3.1. MNSP for Desired Signal SV Estimation

In this subsection, we suppose that the DOA of the desired signal θ_0 lies in the angular region Θ_s, and all DOAs of interference θ_l lie in Θ_l, which is the complement region of Θ_s [3]. For estimating the desired signal SV, we employ MNSP to correct the nominal desired signal SV. Utilizing the orthogonality of noise subspace with incident signal SV [38], MNSP approach minimizing the norm of the projection of SV on the noise subspace estimates the desired signal SV [20]. Eigen-decompose the matrix $\hat{\boldsymbol{R}}$:

$$\begin{aligned} \hat{\boldsymbol{R}} &= \sum\limits_{i=1}^{M} \gamma_i \boldsymbol{u}_i \boldsymbol{u}_i^H = \boldsymbol{U} \boldsymbol{\Gamma} \boldsymbol{U}^H \\ &= \boldsymbol{U}_s \boldsymbol{\Gamma}_s \boldsymbol{U}_s^H + \boldsymbol{U}_n \boldsymbol{\Gamma}_n \boldsymbol{U}_n^H, \end{aligned} \tag{9}$$

where $\gamma_1 \geq \gamma_2 \geq \cdots \gamma_{M-1} \geq \gamma_M$ are the eigenvalues of $\hat{\boldsymbol{R}}$ arranged in descending order [20], and $\boldsymbol{u}_i (i = 1, \ldots, M)$ are eigenvectors of $\hat{\boldsymbol{R}}$ associating with γ_i. γ_M usually considered as a rough estimation of the noise power $\tilde{\sigma}_n^2$ [19]. $\boldsymbol{U}_s = (\boldsymbol{u}_1, \ldots, \boldsymbol{u}_L) \in \mathbb{C}^{M \times L}$ and $\boldsymbol{U}_n = (\boldsymbol{u}_{L+1}, \ldots, \boldsymbol{u}_M) \in \mathbb{C}^{M \times (M-L)}$ consist of L dominant eigenvectors and $M - L$ residual eigenvectors, respectively. Utilizing the eigenvalue-decomposition, we can estimate the column number of $\boldsymbol{U}_s$ quickly by $\min\limits_{L} \frac{\sum_{i=1}^{L} \gamma_i}{\sum_{i=1}^{M} \gamma_i} \leq \zeta$. $\boldsymbol{\Gamma}_s = diag(\gamma_1, \ldots, \gamma_L) \in \mathbb{C}^{M \times L}$ and

$\mathbf{\Gamma}_n = diag(\gamma_{L+1}, \ldots, \gamma_M) \in \mathbb{C}^{M \times (M-L)}$ are eigen-diagonal matrices. According to the properties of the eigen subspace [6], we have:

$$span\{\mathbf{u}_1, \ldots, \mathbf{u}_L\} = span\{\mathbf{a}_0, \ldots, \mathbf{a}_{L-1}\}, \tag{10}$$

where $span\{\mathbf{u}_1, \ldots, \mathbf{u}_L\}$ and $span\{\mathbf{a}_0, \ldots, \mathbf{a}_{L-1}\}$ are signal subspaces spanned by the L dominant eigenvector group $\{\mathbf{u}_1, \ldots, \mathbf{u}_L\}$ and precise signal SV group $\{\mathbf{a}_0, \ldots, \mathbf{a}_{L-1}\}$, respectively. The signal subspace is orthogonal to the noise subspace spanned by $\mathbf{U}_n$ [39]. For any precise SV, $\mathbf{a}_l$ is a linear combination of eigenvector columns $\mathbf{U}_s$ and orthogonal to noise subspace. It means that $\mathbf{U}_n^H \mathbf{a}_l = \mathbf{0}$. However, the SV mismatch destroys its orthogonality and $\mathbf{U}_n^H \mathbf{a}_l = \mathbf{0}$ becomes $\mathbf{U}_n^H \bar{\mathbf{a}}_l \neq \mathbf{0}$. Assume that $\mathbf{e}$ is the mismatch vector between nominal SV and the precise one; precise SV is expressed as $\mathbf{a}_0 = \bar{\mathbf{a}}_0 + \mathbf{e}$ [8]. Therefore, the MNSP approach corrects the $\bar{\mathbf{a}}_l$ by estimating a mismatch vector $\mathbf{e}$ to reestablish the orthogonality between $\mathbf{U}_n^H$ and $\tilde{\mathbf{a}}_l = \bar{\mathbf{a}}_l + \mathbf{e}$. The desired signal SV can be estimated by solving the following optimization problem [14,40]:

$$\begin{aligned}
\min_{\mathbf{e}_\perp} \quad & (\bar{\mathbf{a}}_0 + \mathbf{e}_\perp)^H \mathbf{U}_n \mathbf{U}_n^H (\bar{\mathbf{a}}_0 + \mathbf{e}_\perp) \\
s.t. \quad & \bar{\mathbf{a}}_0^H \mathbf{e}_\perp = 0 \\
& \|(\bar{\mathbf{a}}_0 + \mathbf{e}_\perp)^H \mathbf{U}_n\|_2 \leq \|\bar{\mathbf{a}}_0^H \mathbf{U}_n\|_2 \\
& \|\mathbf{e}_\perp\|_2 \leq \xi,
\end{aligned} \tag{11}$$

where $\mathbf{e}_\perp$ is the orthogonal component of the mismatch vector $\mathbf{e}$ [8]. The parallel component is referred to as $\mathbf{e}_\parallel$. Since $\mathbf{e}_\parallel$ is actually a scaling version of $\bar{\mathbf{a}}_0$, it can be easily proved that $\mathbf{e}_\parallel$ has no impact on output SINR by substituting (7) into (4). Ignoring $\mathbf{e}_\parallel$, the corrected desired signal SV is formulated as $\tilde{\mathbf{a}}_0 = \bar{\mathbf{a}}_0 + \mathbf{e}_\perp$. In (11), the equality constraint is introduced to maintain the orthogonality between $\bar{\mathbf{a}}_0$ and $\mathbf{e}_\perp$ [5,41]. The first inequality constraint is introduced to ensure that $\tilde{\mathbf{a}}_0 = \bar{\mathbf{a}}_0 + \mathbf{e}_\perp$ converges to the desired signal angular region Θ_s. The second inequality constraint is used to limit the $\|\mathbf{e}_\perp\|_2$ to be a small range which guarantees the validity of desired signal SV estimation at low SNR [41]. This optimization problem (11) is a QCQP problem and can be easily solved using a convex optimization toolbox, such as CVX [5,15,19]. Thanks to the idea in [42], we replace $\hat{\mathbf{R}}$ by $\hat{\mathbf{R}}_X = \frac{1}{2}\left(\hat{\mathbf{R}} + \mathbf{I}_V \hat{\mathbf{R}}^* \mathbf{I}_V\right)$ against the coherent scattering mismatch in this paper. $\mathbf{I}_V$ is a $M \times M$ anti-identity matrix. The Hermite's Toeplitz matrix $\hat{\mathbf{R}}_X$ is an unbiased estimation of $\hat{\mathbf{R}}$ [42].

Assume that a signal arrives at a half-wavelength-spaced ULA made up of $M = 10$ sensors from $\theta_0 = 3°$. The values of $\|\mathbf{U}_n^H \mathbf{a}(\theta)\|_2$ and $\|\mathbf{U}_n^H \mathbf{a}(\theta_0)\|_2$ are drawn in Figure 1. It can be observed that the existence of model mismatch destroys the orthogonality of $\mathbf{U}_n$ and $\bar{\mathbf{a}}_0$, and (11) can effectively correct the nominal signal SV $\bar{\mathbf{a}}_0$.
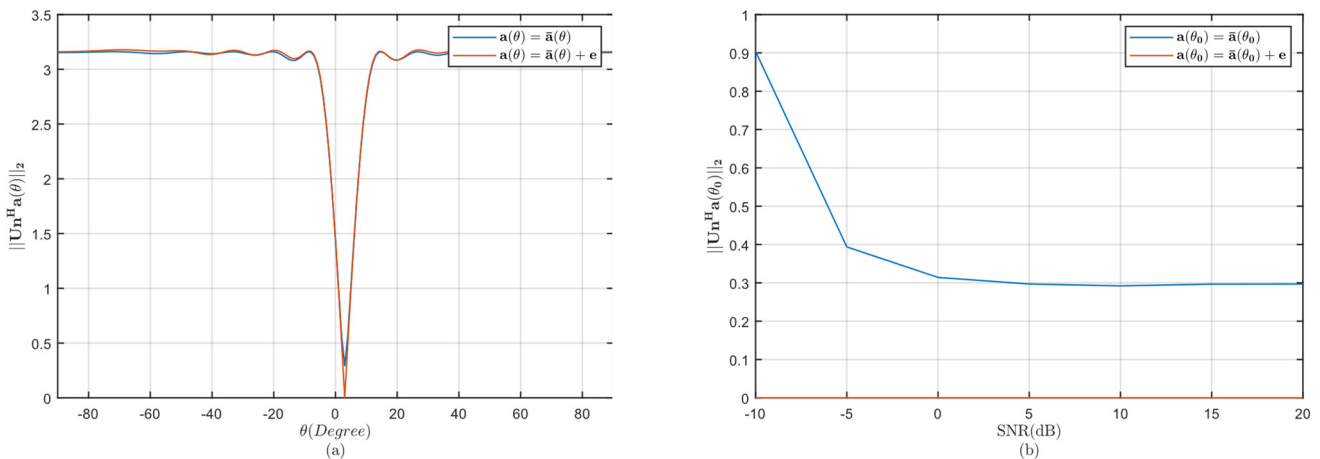

Figure 1. Comparison of (**a**) $\|\mathbf{U}_n^H \mathbf{a}(\theta)\|_2$ versus θ with fixed incident signal $SNR = 5dB$; (**b**) $\|\mathbf{U}_n^H \mathbf{a}(\theta_0)\|_2$ versus incident signal SNR.

3.2. INCM Reconstruction and Beamformer Weight Vector Calculation

To perform INCM reconstruction, the interference SVs and powers need to be estimated first. Based on the advantages of high resolution and low complexity, the maximum entropy power spectrum is adapted to searching each interference DOA in the angular region Θ_l. The maximum entropy power spectrum is written as:

$$\hat{P}_{meps}(\theta) = \frac{1}{\epsilon_p \left| \overline{\boldsymbol{a}}^H(\theta) \hat{\boldsymbol{R}}^{-1} \boldsymbol{u_1} \right|^2}, \theta \in \Theta_l, \tag{12}$$

where $\boldsymbol{u_1} = [1\,0\,\dots 0]^T \in \mathbb{R}^{M \times 1}$, and $\epsilon_p = \frac{1}{\boldsymbol{u_1}^T \hat{\boldsymbol{R}}^{-1} \boldsymbol{u_1}}$. Due to the impact of noise, peaks located in Θ_l may contain some fake peaks that do not correspond to any real interference [19]; $\tilde{\sigma}_n^2$ is set as a threshold for eliminating fake peaks. So far, we obtain P peaks corresponding to interference DOAs by searching J points in Θ_l, and P nominal interference SVs are $\overline{\boldsymbol{a}}_p, p = 1, 2, \dots P$. It has been proved that the Capon, as well as maximum entropy, power spectrum would cause a peak power under-estimation problem [20,43] in the case of model mismatch. We adopt the oblique projection matrix to correct interference SVs for overcoming this drawback.

Given a matrix $\boldsymbol{A} \in \mathbb{C}^{M \times N}(N \leq M)$, $\langle \boldsymbol{A} \rangle$ represents a linear subspace of $\mathbb{C}^M$ spanned by the columns of $\langle \boldsymbol{A} \rangle$ [29], $\boldsymbol{P}_A = \boldsymbol{A}\boldsymbol{A}^+$ represents a projection matrix associated with $\langle \boldsymbol{A} \rangle$, and $\boldsymbol{P}_A^\perp = \boldsymbol{I} - \boldsymbol{P}_A$ represents an orthogonal projection matrix associated with $\langle \boldsymbol{A} \rangle$ [44]. The oblique projection matrix with range space $\langle \boldsymbol{A} \rangle$ and null space $\langle \boldsymbol{B} \rangle$ is denoted by [45]:

$$\boldsymbol{E}_{AB} = \boldsymbol{A} \left(\boldsymbol{A}^H \boldsymbol{P}_{\overline{B}}^\perp \boldsymbol{A} \right)^{-1} \boldsymbol{A}^H \boldsymbol{P}_{\overline{B}}^\perp, \tag{13}$$

where $(\cdot)^+$ represents a pseudo-inverse operator. $\boldsymbol{E}_{AB} \in \mathbb{C}^{M \times M}$ is an idempotent and non-symmetric matrix, and $\boldsymbol{E}_{AB}$ has the following resolution and nulling properties [45]:

$$\boldsymbol{E}_{AB}\boldsymbol{A} = \boldsymbol{A}; \quad \boldsymbol{E}_{AB}\boldsymbol{B} = \boldsymbol{0}; \quad \boldsymbol{P}_{AB} = \boldsymbol{E}_{AB} + \boldsymbol{E}_{BA}. \tag{14}$$

According to the definition of oblique projection, let $\boldsymbol{A} = \boldsymbol{U}_S$, $\boldsymbol{B} = \tilde{\boldsymbol{a}}_0$ and $\boldsymbol{P}_B^\perp = \boldsymbol{I} - \boldsymbol{B}\boldsymbol{B}^+ = \boldsymbol{I} - \boldsymbol{B}(\boldsymbol{B}^H \boldsymbol{B})^{-1} \boldsymbol{B}^H$. The oblique projection matrix associated with interferences is $\boldsymbol{E}_{AB} = \boldsymbol{U}_S \left(\boldsymbol{U}_S^H \boldsymbol{P}_B^\perp \boldsymbol{U}_S \right)^{-1} \boldsymbol{U}_S^H \boldsymbol{P}_B^\perp$. Then, the pth interference SV is corrected as $\tilde{\boldsymbol{a}}_p = \boldsymbol{E}_{AB} \overline{\boldsymbol{a}}_p$, and the power corresponding to the pth interference is obtained by $\tilde{\sigma}_p^2 = \frac{1}{\epsilon_p \left| \tilde{\boldsymbol{a}}_p^H \hat{\boldsymbol{R}}^{-1} \boldsymbol{u_1} \right|^2}$ [46]. The oblique projection is mainly used to correct the nominal interference SV mitigating the impact of desired signal components on the pth interference SV [20,47]. Therefore, the oblique projection can correct interference SVs more accurately compared with orthogonal projection. Based on each corrected interference SV and power, the more precise INCM is reconstructed as (5) [21]:

$$\tilde{\boldsymbol{R}}_{i+n} = \sum_{i=1}^{P} \tilde{\sigma}_i^2 \tilde{\boldsymbol{a}}_i \tilde{\boldsymbol{a}}_i^H + \tilde{\sigma}_n^2 \boldsymbol{I}. \tag{15}$$

Substituting (15) together with $\tilde{\boldsymbol{a}}_0$ calculated by (11) back into the Capon beamformer (7), the proposed method base on INCM reconstruction via oblique projection and desired signal SV estimation via MNSP is written as [6,19]:

$$\tilde{\boldsymbol{w}} = \frac{\tilde{\boldsymbol{R}}_{i+n}^{-1} \tilde{\boldsymbol{a}}_0}{\tilde{\boldsymbol{a}}_0^H \tilde{\boldsymbol{R}}_{i+n}^{-1} \tilde{\boldsymbol{a}}_0}. \tag{16}$$

In our proposed method, computation complexity is principally dominated by calculating and eigen-decomposing the SCM $\hat{\boldsymbol{R}}$, desired signal SV estimation via MNSP, interference peaks searching and interference SVs correction. Calculating the SCM $\hat{\boldsymbol{R}}$ costs

about $O\left((M^2 + M)/2\right)$ flops. Matrix inversion and eigen-decomposition cost about $O(M^3)$ flops. Estimating the desired signal SV via MNSP requires solving a QCQP problem, and the complexity is about $O(M^{3.5})$ flops. The interference peaks searching and interference SV correction cost about $O(max(2MJ, 2M^3))$ flops, where J is the searching points in the angular region of Θ_l [20]. In general, $J < M^2$. Therefore, the overall complexity of this proposed method is roughly $O(max(M^{3.5}, 2M^3))$. By reason of the foregoing, the proposed method is summarized as follows (Method 1):

Method 1. The proposed INCM reconstruction-based RAB method.

1: Calculate the SCM $\hat{\mathbf{R}}$ and $\hat{R}_X$, eigen-decompose $\hat{R}_X$, and obtain $\mathbf{U}_s$, $\mathbf{U}_n$, $\tilde{\sigma}_n^2$;
2: Correct the desired signal SV by solving the QCQP problem (11);
3: Obtain the interference SV estimates $[\bar{\boldsymbol{a}}_1, \ldots, \bar{\boldsymbol{a}}_P]$ using the maximum entropy power spectrum (12);
4: Obtain each corrected interference SV and corresponding power by employing the oblique projection matrix, and reconstruct the INCM via (15);
5: Substitute $\widetilde{\boldsymbol{R}}_{i+n}$ and $\widetilde{\boldsymbol{a}}_0$ back into (7) to obtain the weight vector.

---

4. Numerical Simulation and Analysis

In this section, we perform several numerical simulations under the condition of a half-wavelength ULA with $M = 10$ omnidirectional sensors [6,20]. We assume one desired signal impinging from $\theta_0 = 3°$, two interferences impinging from $\theta_1 = -36°$ and $\theta_2 = 43°$. The additive noise is modeled as a complex circularly symmetric Gaussian zero-mean spatially and temporally white process [5]. All signals, including noise, are assumed to be independent of each other. The input INR is fixed at $INR = 20dB$. In the performance comparison of mean output SINR versus the input SNR [5], the snapshots are set as $K = 100$, and $SNR = 30dB$ in the performance comparison of output SINR versus different snapshots. To obtain each output SINR point, 200 Monte Carlo trials are used [25].

The methods involved in the comparison are as follows: subspace projection and covariance matrix reconstruction (SPCMR) beamformer [20], INCM reconstruction via subspace projection (INCM-SP) beamformer [6], INCM reconstruction and steering vector estimation (INCM-SVE) beamformer [19], INCM reconstruction via orthogonality of subspace (INCM-OS) beamformer [21], INCM reconstruction via the intersection of subspaces (INCM-IS) beamformer [33], INCM reconstruction with iterative mismatch approximation (INCM-IMA) beamformer [3] and INCM reconstruction via power method processing and spatial spectrum matching (PMPSSM) beamformer [48]. Among these methods involved in the comparison, all the angular regions are set as $\Theta_s = \Theta = (\theta_0 - 5°, \theta_0 + 5°)$, $\Theta_l = \overline{\Theta} = (-90°, \theta_0 - 5°) \cup (\theta_0 + 5°, 90°)$ and $\Theta_i = (\theta_i - 5°, \theta_i + 5°)$. The $L = 7$ residual eigenvectors of the matrix C are used, and the boundary of RCB is $\epsilon = \sqrt{0.1}$ in INCM-SVE [6]. The $N = 7$ principal eigenvectors of B are utilized for B_1 in INCM-OS. The constant parameter is $\mu = 0.9$ and $\tau = \sqrt{0.1}$ in SPCMR. The boundaries of amplitude and phase mismatch are set as $\epsilon = 0.3$ and $\Phi = 6°$, the search depth is set as $depth = 10$, and the saturation value is $\varphi = 0.05$ in INCM-SP and INCM-IMA [3]. The number of iterations is set as $k = 4$ in PMPSSM. The determinate threshold $\rho = \rho_l = 0.9$ in INCM-IS. In the proposed method, $\zeta = 0.95$ and $\xi = \sqrt{0.1}$. In the following simulations, the optimal output SINR is calculated by [19]:

$$SINR_{opt} = \sigma_0^2 \boldsymbol{a}_0^H \boldsymbol{R}_{i+n}^{-1} \boldsymbol{a}_0. \tag{17}$$

4.1. Simulation Example 1

In this subsection, we consider the detrimental impact on output SINR of the tested methods when amplitude and phase mismatch existed in the signal model. From the above description, the incident signal SV mismatch is modelled as $\boldsymbol{a}_i = \bar{\boldsymbol{a}}_i + \boldsymbol{e}$, $i = 0, \ldots, L - 1$. To facilitate the analysis, it is indispensable to formally transform the mismatch model of the signal SV. Suppose that α_m and β_m, respectively, represent the amplitude and phase mismatch on mth array-sensor which are extracted from the distribution

$N\left(1, 0.05^2\right)$ and $N\left(0, \left(5°\right)^2\right)$ [19], and the *m*th element of the precise SV is formulated as $a_m = \alpha_m \bar{a}_m e^{j\beta_m}$ [6,19]. The output SINR versus input SNR is delineated in Figure 2a. Our proposed method performs similarly to SPCMR, INCM-SP, INCM-IMA and INCM-SVE at high SNRs. Figure 2b depicts the output SINRs versus snapshot points. The proposed method usually performs better than the other tested methods, and the proposed method can availably resist the finite sampling mismatch [8,36].
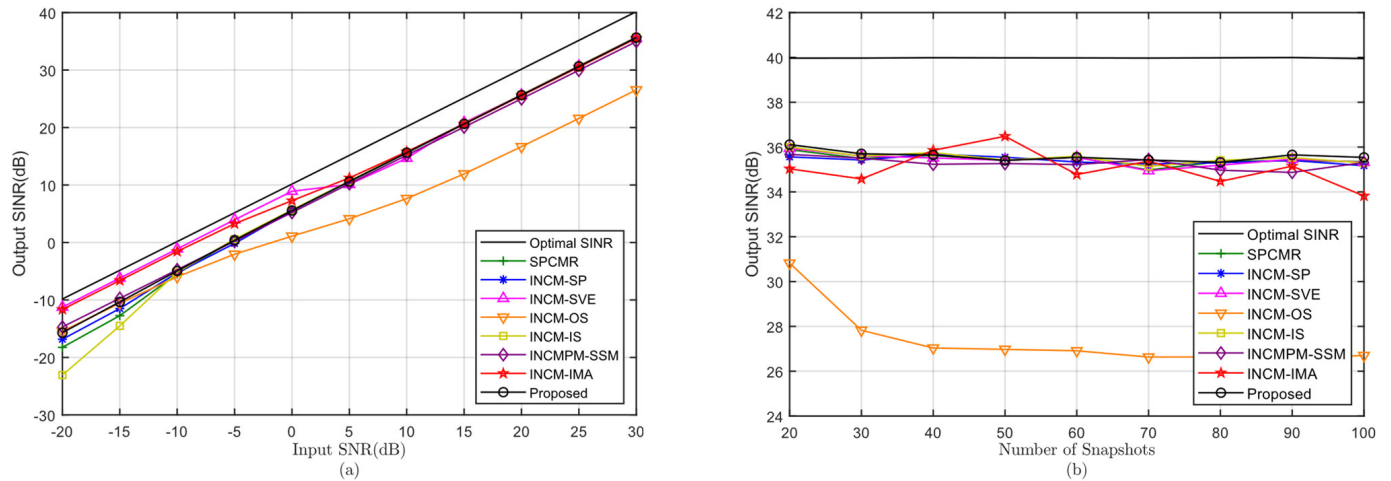

Figure 2. Example 1: output SINR vs.: (**a**) input SNR; (**b**) number of snapshots.

4.2. Simulation Example 2

In this subsection, we consider the detrimental impact on output SINR of the tested methods when random look direction mismatch existed in the signal model. Suppose that the random look direction mismatch of incident signal extracts from uniform distribution $U(-5°, 5°)$ [3]. It is important to note that the amplitude and phase mismatch persist in subsequent simulations. In addition, the random DOAs change in each independent trial while remaining constant over samples [19,31]. The output SINR versus input SNR is delineated in Figure 3a [49]. The performance of our proposed method outperforms other tested methods at high SNRs and is slightly lower than INCM-SVE and INCM-IMA at low SNRs. Figure 3b illustrates that the proposed method outperforms other methods at different snapshots, even with random look direction mismatch.
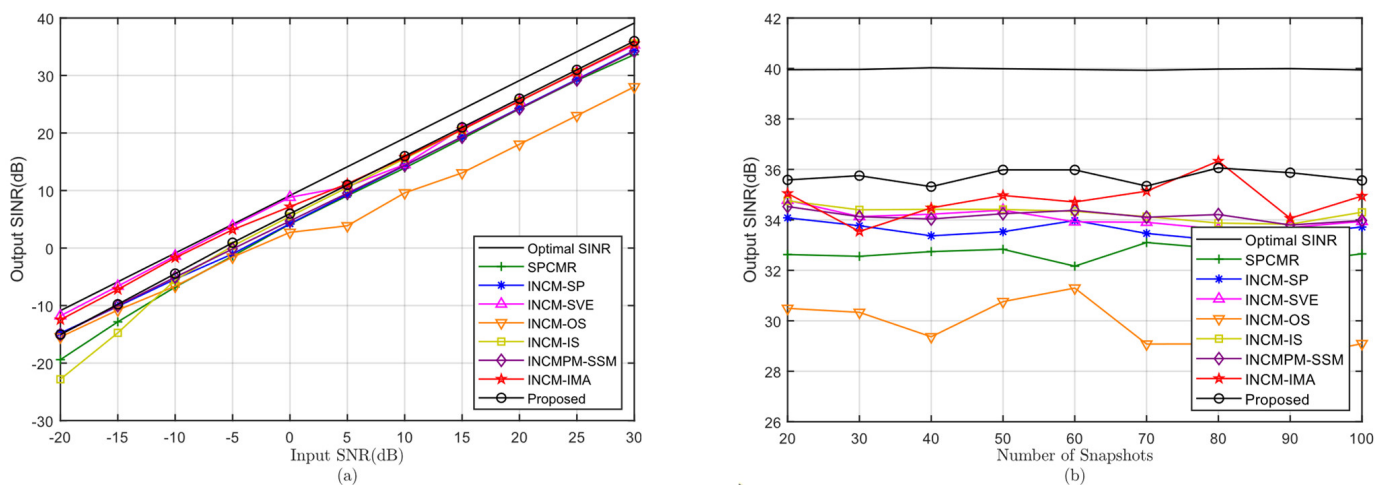

Figure 3. Example 2: output SINR vs.: (**a**) input SNR; (**b**) number of snapshots.

4.3. Simulation Example 3

In this subsection, we consider the detrimental impact on output SINR of the tested methods when incoherent local scattering mismatch existed in the signal model. Suppose that the desired signal has a time-varying signature [7], which is modelled as:

$$\hat{\boldsymbol{x}}_s(k) = s_0(k)\boldsymbol{a}_0 + \sum_{p=1}^{4} s_p(k)\overline{\boldsymbol{a}}(\theta_p),$$ (18)

where $\boldsymbol{a}_0$ and $\overline{\boldsymbol{a}}(\theta_p)$ represent the desired signal SVs corresponding to the direct-path and incoherent scattering paths [21]. In each trial, the DOAs θ_p are independently distributed in a Gaussian distribution drawn from a random generator $N(\theta_0, 4°)$ [6]; $s_p(k)$ are i.i.d zero-mean complex Gaussian random variables drawn from a random generator $N(0, 1)$ [31], and $s_p(k)$ changes both from trial to trial and from sample to sample [19]. Therefore, the rank of desired signal covariance matrix $\boldsymbol{R}_s$ is larger than one, and the output SINR should be expressed as [6]:

$$SINR_{opt} = \frac{\boldsymbol{w}^H \boldsymbol{R}_s \boldsymbol{w}}{\boldsymbol{w}^H \boldsymbol{R}_{i+n} \boldsymbol{w}}.$$ (19)

By maximizing the above SINR in (19), we can obtain the weight vector $\boldsymbol{w}_{opt}$ through the following equation:

$$\boldsymbol{w}_{opt} = P\left\{\boldsymbol{R}_{i+n}^{-1} \boldsymbol{R}_s\right\},$$ (20)

where $P\{\cdot\}$ denotes the prime eigenvector of a matrix [4,8]. In Figure 4a, we can observe that our proposed method has similar performance with INCM-SP, INCM-SVE and INCM-IS at high SNRs and has the best performance at low SNRs. Figure 4b shows the deviations between the tested methods under the conditions of different snapshots. The proposed method obtains the similar output SINR with INCM-SP, INCM-SVE and INCM-IS. Moreover, the IMCMPM-SSM method suffers severe performance degradation in this case.
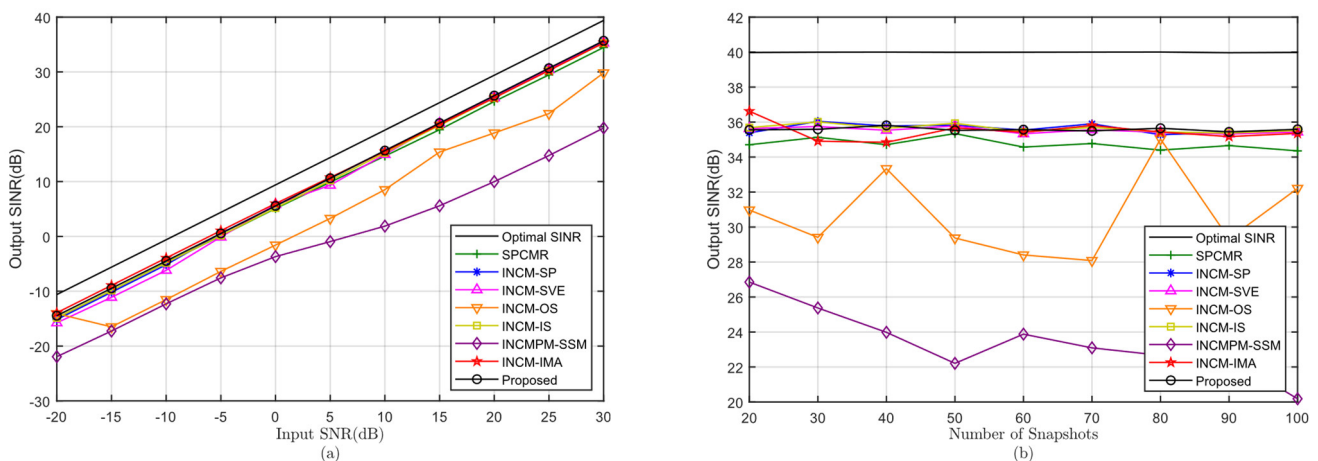

Figure 4. Example 3: output SINR vs.: (**a**) input SNR; (**b**) number of snapshots.

4.4. Simulation Example 4

In this subsection, we consider the detrimental impact on output SINR of the tested methods when coherent local scattering mismatch existed in the signal model. The coherent local scattering mismatch is usually encountered in multipath propagation scenarios [20]. Suppose that the desired signal is distorted by local scattering mismatch and consists of four coherent paths [6]. The precise desired signal SV becomes:

$$\hat{\boldsymbol{a}}_0 = \boldsymbol{a}_0 + \sum_{p=1}^{4} e^{j\phi_p}\overline{\boldsymbol{a}}(\theta_p),$$ (21)

where $\boldsymbol{a}_0$ and $\bar{\boldsymbol{a}}(\theta_p)$ represent desired signal SV and coherent scattering path from θ_p, respectively. In each trial, θ_p, $p = 1, 2, 3, 4$ are independently distributed in a Gaussian distribution drawn from a random generator $N(\theta_0, 4°)$ [6]. The path phases ϕ_p extract from uniform distribution $N(0, 2\pi)$ in each trial. θ_p and ϕ_p remain fixed over the samples [3,6]. Moreover, the norm of $\hat{\boldsymbol{a}}_0$ is no longer equal to $\sqrt{M}$, and optimal output SINR is increased. It can be observed from Figure 5a that the optimal curve has an approximately $6dB$ increment due to the extra coherent scattering paths [3,6]. The performance of our proposed method outperforms other tested methods at high SNRs and is merely lower than INCM-SVE, INCM-IMA and INCMPM-SSM at low SNRs. Figure 5b illustrates that our proposed method generally outperforms others under the condition of finite sampling [8]. Moreover, the IMCMPM-SSM method has good performance compared to the condition of incoherent local scattering mismatch.
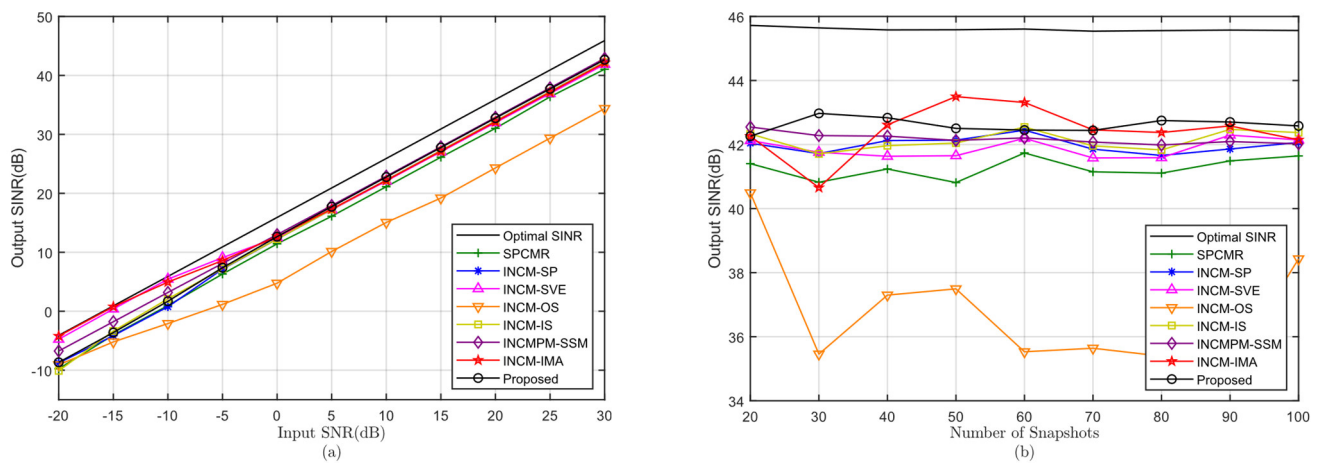

Figure 5. Example 4: output SINR vs.: (**a**) input SNR; (**b**) number of snapshots.

5. Conclusions

This paper utilizes the MNSP approach and established oblique projection matrix to estimate desired signal SV and reconstruct INCM respectively. An MNSP approach minimizes the norm of the projection of SV on the noise subspace to estimate the desired signal SV. An oblique projection matrix is used to alleviate the leakage problem of spatial power spectrum estimation and correct interference SVs. The proposed method can treat various types of SV mismatches while merely requiring a small amount of knowledge about the array configuration and angular region in which the desired signal is located. Multiple simulations are carried out and illustrate that this proposed RAB method performs well and can effectively combat various mismatches.

Author Contributions: All authors have significantly contributed to the research presented in this manuscript; Y.D. presented the main idea and wrote the manuscript; Y.G. edited the manuscript; X.Y. and W.C. reviewed and revised the manuscript. All authors have read and agreed to the published version of the manuscript.

Conflicts of Interest: The authors declare no conflict of interest.

References

1. Vorobyov, S.A.; Gershman, A.B.; Luo, Z.Q. Robust adaptive beamforming using worst-case performance optimization: A solution to the signal mismatch problem. *IEEE Trans. Signal Process.* **2003**, *51*, 313–324. [CrossRef]
2. Du, L.; Li, J.; Stoica, P. Fully Automatic Computation of Diagonal Loading Levels for Robust Adaptive Beamforming. *IEEE Trans. Aerosp. Electron. Syst.* **2010**, *46*, 449–458. [CrossRef]

3. Duan, Y.; Zhang, S.; Cao, W. Covariance matrix reconstruction with iterative mismatch approximation for robust adaptive beamforming. *J. Electromagn. Waves* **2021**, *35*, 2468–2479. [CrossRef]

4. Gu, Y.J.; Goodman, N.A.; Hong, S.H.; Li, Y. Robust adaptive beamforming based on interference covariance matrix sparse reconstruction. *Signal Process.* **2014**, *96*, 375–381. [CrossRef]

5. Gu, Y.J.; Leshem, A. Robust Adaptive Beamforming Based on Interference Covariance Matrix Reconstruction and Steering Vector Estimation. *IEEE Trans. Signal Process.* **2012**, *60*, 3881–3885. [CrossRef]

6. Duan, Y.L.; Yu, X.H.; Mei, L.R.; Cao, W.P. Low-Complexity Robust Adaptive Beamforming Based on INCM Reconstruction via Subspace Projection. *Sensors* **2021**, *21*, 7783. [CrossRef] [PubMed]

7. Zhu, X.Y.; Ye, Z.F.; Xu, X.; Zheng, R. Covariance Matrix Reconstruction via Residual Noise Elimination and Interference Powers Estimation for Robust Adaptive Beamforming. *IEEE Access* **2019**, *7*, 53262–53272. [CrossRef]

8. Huang, L.; Zhang, J.; Xu, X.; Ye, Z. Robust Adaptive Beamforming With a Novel Interference-Plus-Noise Covariance Matrix Reconstruction Method. *IEEE Trans. Signal Process.* **2015**, *63*, 1643–1650. [CrossRef]

9. Li, J.; Stoica, P.; Wang, Z.S. Doubly constrained robust Capon beamformer. *IEEE Trans. Signal Process.* **2004**, *52*, 2407–2423. [CrossRef]

10. Vorobyov, S.A.; Rong, Y.; Gershman, A.B. Robust adaptive beamforming using probability-constrained optimization. In Proceedings of the 2005 IEEE/SP 13th Workshop on Statistical Signal Processing (SSP), Bordeaux, France, 17–20 July 2005; Volumes 1–2, pp. 869–874.

11. Vorobyov, S.A.; Chen, H.H.; Gershman, A.B. On the Relationship Between Robust Minimum Variance Beamformers With Probabilistic and Worst-Case Distortionless Response Constraints. *IEEE Trans. Signal Process.* **2008**, *56*, 5719–5724. [CrossRef]

12. Liu, J.B.; Gui, G.; Xie, W.; Cong, X.C.; Wan, Q.; Adachi, F. Robust Widely Linear Beamforming via an IAA Method for the Augmented IPNCM Reconstruction. *IEICE Trans. Fundam. Electron.* **2017**, *E100a*, 1562–1566. [CrossRef]

13. Huang, F.; Sheng, W.X.; Ma, X.F. Modified projection approach for robust adaptive array beamforming. *Signal Process.* **2012**, *92*, 1758–1763. [CrossRef]

14. Jia, W.M.; Jin, W.; Zhou, S.H.; Yao, M.L. Robust adaptive beamforming based on a new steering vector estimation algorithm. *Signal Process.* **2013**, *93*, 2539–2542. [CrossRef]

15. Huang, L.; Zhang, B.; Ye, Z.F. Robust Adaptive Beamforming Using a New Projection Approach. In Proceedings of the 2015 IEEE International Conference on Digital Signal Processing (DSP), Singapore, 21–24 July 2015; pp. 1181–1185.

16. Yu, Z.L.; Gu, Z.H.; Zhou, J.J.; Li, Y.Q.; Ser, W.; Er, M.H. A Robust Adaptive Beamformer Based on Worst-Case Semi-Definite Programming. *IEEE Trans. Signal Process.* **2010**, *58*, 5914–5919. [CrossRef]

17. Beck, A.; Eldar, Y.C. Doubly constrained robust capon beamformer with ellipsoidal uncertainty sets. *IEEE Trans. Signal Process.* **2007**, *55*, 753–758. [CrossRef]

18. Jiang, X.; Zeng, W.J.; Yasotharan, A.; So, H.C.; Kirubarajan, T. Robust Beamforming by Linear Programming. *IEEE Trans. Signal Process.* **2014**, *62*, 1834–1849. [CrossRef]

19. Zheng, Z.; Zheng, Y.; Wang, W.Q.; Zhang, H.B. Covariance Matrix Reconstruction With Interference Steering Vector and Power Estimation for Robust Adaptive Beamforming. *IEEE Trans. Veh. Technol.* **2018**, *67*, 8495–8503. [CrossRef]

20. Ai, X.Y.; Gan, L. Robust Adaptive Beamforming With Subspace Projection and Covariance Matrix Reconstruction. *IEEE Access* **2019**, *7*, 102149–102159. [CrossRef]

21. Zhu, X.; Xu, X.; Ye, Z. Robust adaptive beamforming via subspace for interference covariance matrix reconstruction. *Signal Process.* **2020**, *167*, 107289. [CrossRef]

22. Chen, P.; Yang, Y.X. An uncertainty-set-shrinkage-based covariance matrix reconstruction algorithm for robust adaptive beamforming. *Multidimens. Syst. Signal Process.* **2021**, *32*, 263–279. [CrossRef]

23. Mallipeddi, R.; Lie, J.P.; Suganthan, P.N.; Razul, S.G.; See, C.M.S. Robust adaptive beamforming based on covariance matrix reconstruction for look direction mismatch. *PIER Lett.* **2011**, *25*, 34–46. [CrossRef]

24. Ruan, H.; de Lamare, R.C. Robust Adaptive Beamforming Using a Low-Complexity Shrinkage-Based Mismatch Estimation Algorithm. *IEEE Signal Process. Lett.* **2014**, *21*, 60–64. [CrossRef]

25. Shen, F.; Chen, F.F.; Song, J.Y. Robust Adaptive Beamforming Based on Steering Vector Estimation and Covariance Matrix Reconstruction. *IEEE Commun. Lett.* **2015**, *19*, 1636–1639. [CrossRef]

26. Mohammadzadeh, S.; Nascimento, V.H.; Lamare, R.C.d.; Kukrer, O. Maximum Entropy-Based Interference-Plus-Noise Covariance Matrix Reconstruction for Robust Adaptive Beamforming. *IEEE Signal Process. Lett.* **2020**, *27*, 845–849. [CrossRef]

27. Mohammadzadeh, S.; Nascimento, V.H.; Lamare, R.C.d.; Kukrer, O. Low-Cost Adaptive Maximum Entropy Covariance Matrix Reconstruction for Robust Beamforming. In Proceedings of the 2020 54th Asilomar Conference on Signals, Systems, and Computers, California, CA, USA, 1–4 November 2020; pp. 1462–1466.

28. Zhang, Y.P.; Li, Y.J.; Gao, M.G. Robust adaptive beamforming based on the effectiveness of reconstruction. *Signal Process.* **2016**, *120*, 572–579. [CrossRef]

29. Zhuang, J.; Manikas, A. Interference cancellation beamforming robust to pointing errors. *IET Signal Process.* **2013**, *7*, 120–127. [CrossRef]

30. Zhang, X.-J.; Feng, D.-Z.; Nie, W.-K.; Lin, S.-Y.; Hu, H.-S. Robust adaptive beamforming algorithm based on damped singular value decomposition regularization. *Digit. Signal Process.* **2022**, *122*, 103356. [CrossRef]

31. Zheng, Z.; Yang, T.; Wang, W.Q.; So, H.C. Robust Adaptive Beamforming via Simplified Interference Power Estimation. *IEEE Trans. Aerosp. Electron. Syst.* **2019**, *55*, 3139–3152. [CrossRef]

32. Shao, X.; Hu, T.; Zhang, J.; Pan, Y.; Zhang, Z.; Wei, Y. A low-sidelobe adaptive beamforming algorithm with single snapshot. In Proceedings of the IET International Radar Conference (IET IRC 2020), Chongqing, China, 4–6 November 2020; pp. 682–686.

33. Wang, R.; Wang, Y.; Han, C.; Gong, Y.; Wang, L. Robust Adaptive Beamforming Based on Interference Covariance Matrix Reconstruction and Steering Vector Estimation. In Proceedings of the 2021 IEEE International Conference on Signal Processing, Communications and Computing (ICSPCC), Xi'an, China, 17–19 August 2021; pp. 1–5.

34. Liao, B.; Chan, S.C.; Tsui, K.M. Recursive Steering Vector Estimation and Adaptive Beamforming under Uncertainties. *IEEE Trans. Aerosp. Electron. Syst.* **2013**, *49*, 489–501. [CrossRef]

35. Gu, Y.J.; Shi, Z.G.; Chen, K.S.; Li, Y. Robust adaptive beamforming for steering vector uncertainties based on equivalent DOAs method. *Prog. Electromagn. Res.* **2008**, *79*, 277–290. [CrossRef]

36. Huang, J.S.; Su, H.T.; Yang, Y. Low-complexity robust adaptive beamforming method for MIMO radar based on covariance matrix estimation and steering vector mismatch correction. *IET Radar Sonar Navig.* **2019**, *13*, 712–720. [CrossRef]

37. Xie, Z.; Zhu, J.H.; Fan, C.Y.; Huang, X.T. An Improved Sub-Array Adaptive Beamforming Technique Based on Multiple Sources of Errors. *J. Mar. Sci. Eng.* **2020**, *8*, 757. [CrossRef]

38. Lee, J.H.; Cheng, K.P.; Wang, C.C. Robust adaptive array beamforming under steering angle mismatch. *Signal Process.* **2006**, *86*, 296–309. [CrossRef]

39. Xu, X.; Ye, Z.F.; Zhang, Y.F. DOA Estimation for Mixed Signals in the Presence of Mutual Coupling. *IEEE Trans. Signal Process.* **2009**, *57*, 3523–3532. [CrossRef]

40. Yang, B.; Li, W.X.; Li, Y.Y.; Zhang, Q. Robust adaptive null broadening beamforming based on subspace projection. *Int. J. Electron.* **2022**, 1–15. [CrossRef]

41. Gong, C.; Huang, L.; Xu, D.; Ye, Z. Knowledge-aided robust adaptive beamforming with small snapshots. *Electron. Lett.* **2013**, *49*, 1258–1259. [CrossRef]

42. Du, Y.; Cui, W.; Mei, F.; Xu, H.; Wang, Y. Coherent signals adaptive beamforming algorithm based on eigenvalue. In Proceedings of the 2021 2nd International Conference on Electronics, Communications and Information Technology (CECIT), Sanya, China, 27–29 December 2021; pp. 388–393.

43. Stoica, P.; Li, J.; Tan, X. On spatial power spectrum and signal estimation using the Pisarenko framework. *IEEE Trans. Signal Process.* **2008**, *56*, 5109–5119. [CrossRef]

44. Chen, P.; Zuo, L.; Wang, W. Adaptive Beamforming for Passive Synthetic Aperture with Uncertain Curvilinear Trajectory. *Remote Sens.* **2021**, *13*, 2562. [CrossRef]

45. McCloud, M.L.; Scharf, L.L. A new subspace identification algorithm for high-resolution DOA estimation. *IEEE Trans. Antennas Propag.* **2002**, *50*, 1382–1390. [CrossRef]

46. Yang, B.; Li, W.X.; Li, Y.Y.; Yue, C.Y. Novel robust adaptive beamforming against unknown mutual coupling. *J. Electromagn. Waves* **2021**, *35*, 2447–2467. [CrossRef]

47. Yang, X.P.; Li, Y.Q.; Liu, F.F.; Lan, T.; Long, T.; Sarkar, T.K. Robust Adaptive Beamforming Based on Covariance Matrix Reconstruction With Annular Uncertainty Set and Vector Space Projection. *IEEE Antennas Wirel. Propag. Lett.* **2021**, *20*, 130–134. [CrossRef]

48. Mohammadzadeh, S.; Nascimento, V.H.; Lamare, R.C.D.; Kukrer, O. Robust Adaptive Beamforming Based on Power Method Processing and Spatial Spectrum Matching. In Proceedings of the ICASSP 2022—2022 IEEE International Conference on Acoustics, Speech and Signal Processing (ICASSP), Singapore, 23–27 May 2022; pp. 4903–4907.

49. Lu, J.; Yang, J.; Yao, Z.C.; Zhu, F.C.; Yu, Z.Y.; Liu, G.B. Robust wideband adaptive beamforming based on covariance matrix reconstruction in the spatial-frequency domain. *IET Microw. Antennas Propag.* **2021**, *15*, 309–322. [CrossRef]